# Self-Lubricating and Self-Healing Polyurethane Nanocomposites Based on Aminated-Ti$_3$C$_2$T$_x$

Chunpeng Chai,* Zhenqian Ma, Xuan Yin, and Haosheng Pang*

Read Online

ACCESS | Metrics & More | Article Recommendations

**ABSTRACT:** Self-healing polyurethane is a matrix material that can effectively extend the service life of composite materials. The layered two-dimensional Ti$_3$C$_2$T$_x$ material has weak interlayer van der Waals forces, which can undergo slip and form transfer films during friction, reducing shear strength and improving the lubrication performance of the material. Therefore, we introduced two-dimensional Ti$_3$C$_2$T$_x$ into a self-healing polyurethane matrix to improve the lubrication performance of the matrix material. A dual-ion self-healing polyurethane (SPU) was prepared using N-methyl diethanolamine, hexamethylene diisocyanate, and 1,3-propane sultone as raw materials. Ti$_3$C$_2$T$_x$ was prepared by chemical etching, and NH$_2$−Ti$_3$C$_2$T$_x$ was obtained by chemically grafting amino groups onto the surface of Ti$_3$C$_2$T$_x$ using aminopropyltriethoxysilane. Then, it was mixed into the SPU matrix to obtain the NH$_2$−Ti$_3$C$_2$T$_x$/SPU composite material. Compared with pure SPU, the friction coefficient and wear rate of the system were reduced by 79.7% and 97.8%, respectively. Under 75%RH and 20 °C conditions, self-healing could be achieved rapidly within 5 min, with a self-healing efficiency of 84.4%. The kind of self-lubricating and self-healing polyurethane modified by amination-Ti$_3$C$_2$T$_x$ is expected to be applied in automotive, electronics, and biomedicine.

**KEYWORDS:** polyurethane, MXenes, surface modification, self-healing, self-lubrication
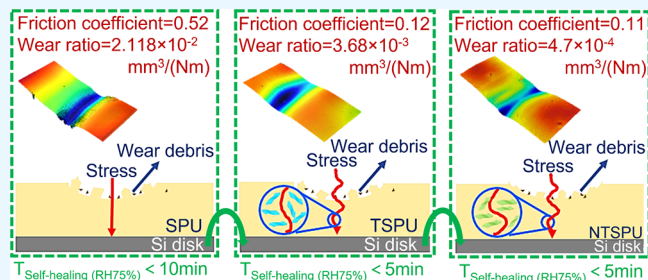
## 1. INTRODUCTION

Lubricating materials refer to substances that can reduce friction and wear and have specific physical and chemical properties.[1,2] They are widely used in various fields, such as automotive, aerospace, electronics, and biomedicine. With the development of society and the advancement of science and technology, higher requirements have been put forward for reducing mechanical wear, reducing energy consumption, and extending the service life of mechanical components.[3] It is well-known that efficient lubricating materials are essential for the stable operation and energy savings of mechanical systems. Pioneers' research on lubricating materials is crucial.[4−7] Polymer materials, due to their characteristics of "lightweight, low cost, excellent corrosion resistance, good self-lubrication, and adjustable structure", are considered to be good matrix materials in the field of solid lubrication. The most commonly used polymer matrix materials include polytetrafluoroethylene (PTFE), polyimide (PI), poly(phenylene sulfide) (PPS), and polyurethane (PU). Although PTFE has a low friction coefficient, excellent chemical stability, and good biocompatibility, its wear rate is high under high loads.[8,9] PI is a high-performance engineering plastic with excellent high-temperature resistance, mechanical properties, and creep resistance, but its friction coefficient and wear rate are relatively high.[10,11]

PPS has excellent corrosion resistance, high-temperature resistance, and radiation resistance, but its brittleness and low impact strength limit its application range.[12] Polyurethane, with its structure containing hard and soft segments, has a diverse structure and design flexibility, making its performance adjustable and suitable for various application scenarios.[13−16] It has a relatively low friction coefficient and wear rate among many polymer matrix materials, making it one of the most promising polymer matrices in the field of solid lubrication.[17,18] With the advancement of modern science and technology, higher requirements have been proposed for polyurethane-based solid lubricating composite film materials, namely, to improve the lubrication performance of materials based on extending the service life of materials and reducing energy consumption.[19−22] To extend the service life of polyurethane-based composite film materials, choosing a self-healing polyurethane with a self-healing function as the matrix
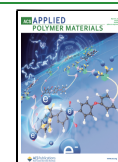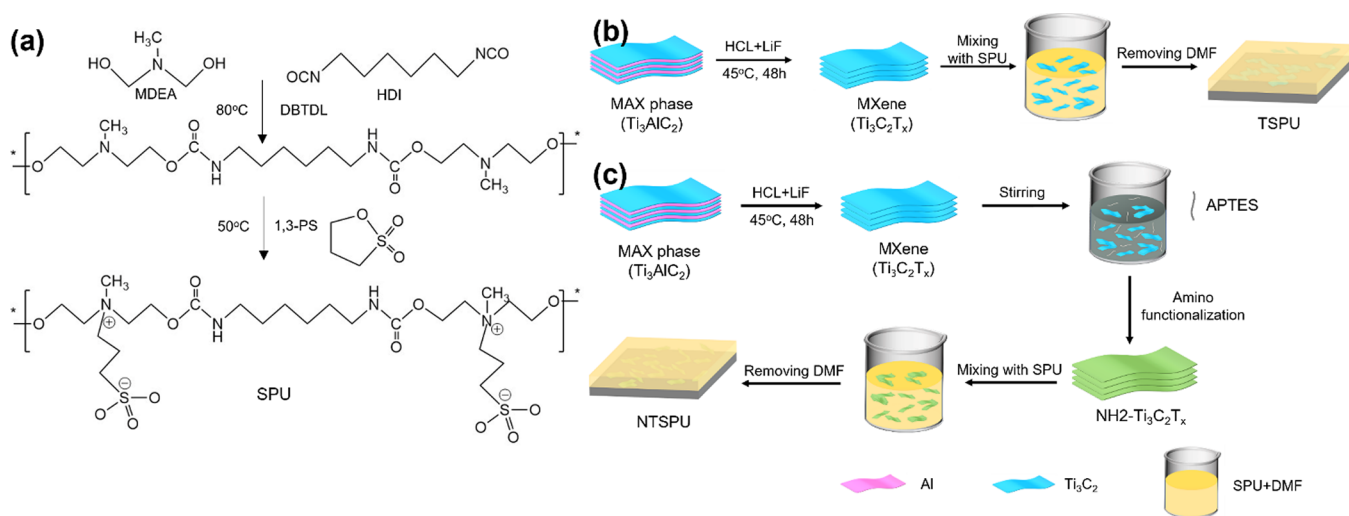
**Figure 1.** Synthesis diagram of (a) SPU, (b) TSPU, and (c) NTSPU.

of the composite film material is an effective approach.[23−25] It is worth noting that compatibility with self-lubrication and self-healing is the key to realizing long-life coating for automotive and aerospace devices. Dual-ion polyurethane has a large number of ion structures, which can form physical cross-links between these ion structures and interact with each other to produce reversible cross-linked ion clusters.[26,27] Under certain conditions, the ion clusters can reform a network structure, thereby achieving self-healing of damaged parts of the material.[28−30] To improve the lubrication performance of the material, new and efficient solid lubricant additives can be added to the self-healing polyurethane matrix.

The two-dimensional material $Ti_3C_2T_x$, due to its unique layered structure, strong intralayer chemical bonds, and weak interlayer forces, is prone to slip between layers during friction and forms a self-lubricating transfer film at the friction interface.[31−33] Therefore, $Ti_3C_2T_x$ shows great potential in the field of solid lubrication and can act as an efficient lubricant additive in composite film materials.[34,35] However, $Ti_3C_2T_x$ has poor dispersion in the matrix and is prone to agglomeration and clustering.[36,37] Therefore, it is of great significance to modify $Ti_3C_2T_x$ to improve its dispersion in the matrix. Studies have shown that the functional modification of $Ti_3C_2T_x$ by adjusting the surface terminal functional groups can promote its interaction with the polymer matrix interface. Grafting amino groups ($-NH_2$) on the $Ti_3C_2T_x$ surface is a simple and effective method to promote the interaction between $Ti_3C_2T_x$ and the matrix material interface.[38] For example, the research group led by Professor Xiaoqiang Fan[39] from Southwest Jiaotong University modified $Ti_3C_2T_x$ using 3-aminopropyltriethoxysilane (APTES) to prepare amino-functionalized $Ti_3C_2T_x$ (f-$Ti_3C_2$), which was then compounded with waterborne epoxy resin (EP) to obtain f-$Ti_3C_2$/EP composite film materials. The study showed that due to the interaction between amino and epoxy groups, f-$Ti_3C_2$ could maintain a uniform and stable state in the epoxy resin slurry for 30 days, and the composite film material with 0.5 wt % f-$Ti_3C_2$ had the best tribological performance, with an average friction coefficient of 0.357 and a wear rate of $1.93 \times 10^{-4}$ mm$^3$/(Nm). The research group[40] further compounded amino-functionalized $Ti_3C_2T_x$ (k-$Ti_3C_2$) with an interpenetrating polymer network (IPN) to obtain k-$Ti_3C_2$/IPN composite film materials. The study showed that the interface interaction

between amino-functionalized $Ti_3C_2T_x$ and IPN was enhanced, and the k-$Ti_3C_2$ nanosheets maintained a uniform and stable dispersion in the coating, effectively reducing the wear rate of the material. In addition, it was found that APTES modification could not only effectively prevent the stacking of $Ti_3C_2T_x$ layers but also act as a protective layer, effectively preventing the oxidation of $Ti_3C_2T_x$ in oxygen and water environments. Therefore, APTES modification is an effective method to enhance the interaction between $Ti_3C_2T_x$ and the matrix material interface and to improve its dispersion.

This study first prepared two-dimensional material $Ti_3C_2T_x$ using the chemical etching method, and then modified $Ti_3C_2T_x$ with silane coupling agent APTES to obtain amino-functionalized $Ti_3C_2T_x$ ($NH_2-Ti_3C_2T_x$). Self-healing polyurethane (SPU) was synthesized using a two-step method, and a physical blending method was used to composite SPU with $Ti_3C_2T_x$ and $NH_2-Ti_3C_2T_x$, resulting in $Ti_3C_2T_x$/SPU composite film material TSPU and $NH_2-Ti_3C_2T_x$/SPU composite film material NTSPU. The structure and composition of $NH_2-Ti_3C_2T_x$ and composite film materials were characterized using spectroscopy and energy spectrum. The thermal, mechanical, lubrication, and self-healing properties, of TSPU and NTSPU were studied using a universal mechanical testing machine, metallographic microscope, multifunctional friction tester, and three-dimensional profilometer.

## 2. EXPERIMENT

**2.1. Materials.** *N*-Methyldiethanolamine, 99%, Shanghai Aladdin Biochemical Technology Co., Ltd. Hexamethylene diisocyanate, 99%, Shanghai Mayer Chemical Technology Co., Ltd. 1,3-Propane sultone, 99%, Shanghai Aladdin Biochemical Technology Co., Ltd. N, N-dimethylformamide, analytical grade, Beijing Tongguang Fine Chemical Co., Ltd. Dibutyltin dilaurate, 95%, Alpha Aesar (China) Chemical Co., Ltd. Ti3AlC2, 98%, Jilin Province Yiyi Technology Co., Ltd. Lithium fluoride (99%), Shanghai Mayer Chemical Technology Co., Ltd. Hydrochloric acid, analytical grade, Beijing Tongguang Fine Chemical Co., Ltd. Anhydrous ethanol, analytical grade, Beijing Tongguang Fine Chemical Co., Ltd. 3-Aminopropyltriethoxysilane, 99%, Shanghai Aladdin Biochemical Technology Co., Ltd.

**2.2. Methods.** *2.2.1. Synthesis of $NH_2-Ti_3C_2T_x$.* Add 1 g of lithium fluoride to a polypropylene plastic bottle containing 20

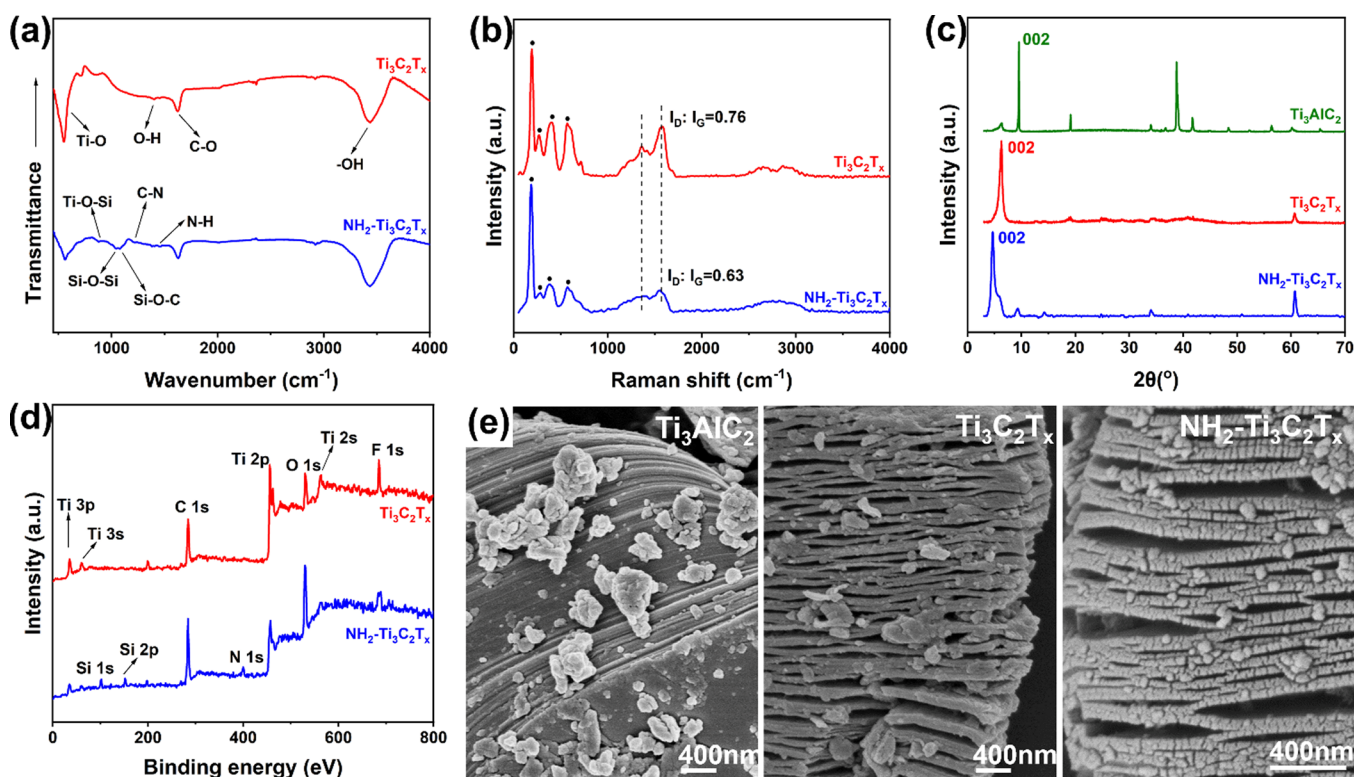**Figure 2.** Microstructure and chemical constitution of $Ti_3C_2T_x$ and $NH_2-Ti_3C_2T_x$ sheets. (a) FTIR spectra. (b) Raman spectra. (c) XRD spectra. (d) XPS spectra. (e) SEM of $Ti_3AlC_2$, $Ti_3C_2T_x$, and $NH_2-Ti_3C_2T_x$ sheets.

mL of 9 mol/L hydrochloric acid and stir continuously for 0.5 h to ensure complete dissolution of the lithium fluoride. Slowly add 1 g of $Ti_3AlC_2$ to the hydrochloric acid solution containing dissolved lithium fluoride, and then etch continuously at 45 °C and 400 rpm for 48 h. Afterward, the etched product was rinsed with deionized water until the pH of the supernatant was ≥6. Finally, dry the $Ti_3C_2T_x$ at 60 °C for 48 h in an oven to obtain $Ti_3C_2T_x$. In a mixture of 36 g of ethanol and 4 g of deionized water, 10 g of APTES was added and stirred thoroughly until dissolved. Add 0.5 g of $Ti_3C_2T_x$ to the above mixture and sonicate for 1 h. Then the mixture was transferred to a 250 mL round-bottom flask and stirred at 80 °C under reflux conditions for 24 h. Wash the reaction residue multiple times with a mixture of ethanol and deionized water (mass ratio of 9:1), and finally dry at 60 °C in an oven for 48 h to obtain $NH_2-Ti_3C_2T_x$.

*2.2.2. Synthesis of PU matrix (SPU).* First, 5.958 g of *N*-Methyldiethanolamine (MDEA) was weighed and poured into a 500 mL round-bottom flask. Measure 65 mL of N,N-dimethylformamide (DMF) and add it to the flask. Fix the round-bottom flask on an iron stand, install a stirrer, set the temperature to 80 °C, and stir for 10 min to completely dissolve the MDEA in DMF. Then weigh 8.82 g of HDI and add it to the system, along with 0.5 wt % dibutyltin dilaurate (DBTDL). React at 80 °C for 6 h to complete the prepolymerization. Finally, the temperature of the oil bath was adjusted to 50 °C; 4.884 g of 1,3-Propane sultone (1,3-PS), added to the system, and reacted at 50 °C for 8 h to obtain the SPU solution. The preparation principle of SPU is shown in Figure 1.

*2.2.3. Synthesis of PU-Based Composites. 2.2.3.1. $Ti_3C_2T_x$/ SPU Composites (TSPU).* As shown in Figure 1, first a certain amount of SPU solution is weighed, and then the

corresponding mass fractions of $Ti_3C_2T_x$ (0.25, 0.50, 0.75, 1.00, 1.25, 1.50 wt %). Dissolve the measured $Ti_3C_2T_x$ in 2 mL of DMF and sonicate for 2 h to obtain a $Ti_3C_2T_x$ dispersion. Then add the dispersion to the SPU solution and stir for 3 h to obtain the $Ti_3C_2T_x$/SPU solution. Finally, the solution was spin-coated to form a film and dried at 60 °C in an oven for 48 h to obtain a $Ti_3C_2T_x$/SPU composite film (TSPU), denoted as TSPU-0.25, TSPU-0.50, TSPU-0.75, TSPU-1.00, TSPU-1.25, and TSPU-1.50.

*2.2.3.2. $NH_2-Ti_3C_2T_x$/SPU Composites (NTSPU).* Weigh a certain amount of SPU solution and then weigh the corresponding mass fractions of $NH_2-Ti_3C_2T_x$ (0.25, 0.50, 0.75, 1.00, 1.25, 1.50 wt %). Dissolve the measured $NH_2-Ti_3C_2T_x$ in 2 mL of DMF and sonicate for 2 h to obtain an $NH_2-Ti_3C_2T_x$ dispersion. Then the dispersion was added to the SPU solution and stirred for 3 h to obtain the $NH_2-Ti_3C_2T_x$/SPU solution. Finally, the solution was spin-coated to form a film and dried at 60 °C in an oven for 48 h to obtain $NH_2-Ti_3C_2T_x$/SPU composite film (NTSPU), denoted as NTSPU-0.25, NTSPU-0.50, NTSPU-0.75, NTSPU-1.00, NTSPU-1.25, and NTSPU-1.50 (Figure 1).

**2.3. Characterizations.** *2.3.1. Structure and Morphology.* The microstructure of $NH_2-Ti_3C_2T_x$ was characterized using a JEOL transmission electron microscope (TEM) model JEM-F200. The functional group structures of $Ti_3C_2T_x$ and $NH_2-Ti_3C_2T_x$ were characterized using a Fourier-transform infrared (FTIR) spectrometer model INVENIO from Bruker in Germany. The crystal structures of $Ti_3AlC_2$, $Ti_3C_2T_x$, and $NH_2-Ti_3C_2T_x$ were characterized using an X-ray diffractometer model D8 ADVANCE from Bruker in Germany. The scan angle range was 3−70° with a 5°/min scan rate by using a Cu target. The degree of carbon ordering in $Ti_3C_2T_x$ and $NH_2-Ti_3C_2T_x$ was characterized using a Raman spectrometer model
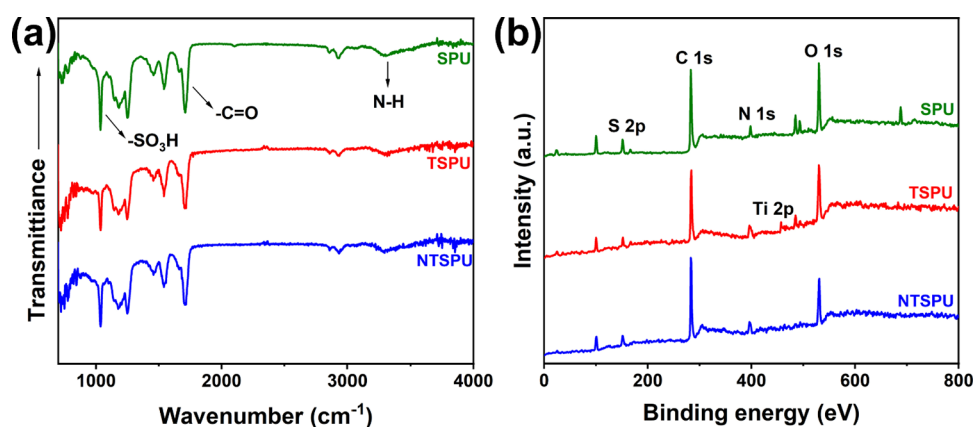
**Figure 3.** Chemical constitution of PU-based composites. (a) FTIR spectra. (b) XPS spectra.

HR Evolution from Horiba in Japan. The friction surfaces of $Ti_3C_2T_x$, $NH_2-Ti_3C_2T_x$, and $NH_2-Ti_3C_2T_x$/SPU composite film materials were characterized using an X-ray photoelectron spectroscopy (XPS) instrument model PHI QUANTERA-II SXM from ULVAC-PHI in Japan. An Al target was used. The excitation wavelength was 532 cm$^{-1}$, and the scanning range was 50−4000 cm$^{-1}$. The microstructure and elemental distribution of $Ti_3C_2T_x$, $NH_2-Ti_3C_2T_x$, and $NH_2-Ti_3C_2T_x$/SPU composite film materials were characterized using a scanning electron microscope (SEM) model Gemini 300 from the ZEISS Group in Germany.

*2.3.2. Mechanical Property.* The mechanical properties of the samples were tested using an electronic universal testing machine model AGS-J from Shimadzu in Japan. According to the GB/T528-1998 method, the samples were prepared into dumbbell-shaped specimens. The testing temperature was 20 °C, and the tensile rate was set at 100 mm/min.

*2.3.3. Tribological Property.* ==The material was subjected to a rotational friction test using a multifunctional friction tester model MS-M9000 from Lanzhou Huahui Instrument Technology Co., Ltd. The friction coefficient of the material was obtained.== The test was conducted with a load of 3N, while the $Si_3N_4$ ball rubbed against the coatings for 1000s at a speed of 60 r/min and a friction radius of 3 mm. Please note that the specific calculation method may vary depending on the experimental conditions and material properties. It is recommended to refer to the operation manual of the instrument and experimental method for accurate calculation methods:

$$W = V/(F \times L) \tag{1}$$

In the equation, $W$ (mm$^3$ N$^{-1}$ m$^{-1}$) represents the wear rate, $V$ (mm$^3$) represents the wear volume, $F$ (N) represents the applied load, and $L$ (m) represents the total travel distance.

*2.3.4. Self-Healing Property.* According to the GB/T528-1998 method, dumbbell-shaped specimens were prepared. The specimens were cut in the middle section. Without any additives or external energy, the cut specimens were placed in a constant temperature and humidity chamber at 30%RH and 75%RH, 20 °C. The healing process was observed using a GP-200MRT metallographic microscope. Please note that the specific equations for calculating the self-healing efficiency may vary depending on the experimental setup and parameters. It is recommended to refer to the relevant literature or experimental protocol for an accurate calculation method:

$$\eta_\sigma = \sigma_r/\sigma_0 \tag{2}$$

In the equation, $\sigma_r$ represents the tensile strength of the healed specimen, and $\sigma_0$ represents the tensile strength of the initial specimen.

## 3. RESULTS AND DISCUSSION

**3.1. Compositions of $NH_2-Ti_3C_2T_x$ and PU-Based Composites.** *3.1.1. Compositions of $NH_2-Ti_3C_2T_x$.* The structure and composition of $NH_2-Ti_3C_2T_x$ were characterized by using FT-IR, as shown in Figure 2a. $Ti_3C_2T_x$ and $NH_2-Ti_3C_2T_x$ share some common chemical groups. The FT-IR peaks at 3437, 1624, 1399, and 554 cm$^{-1}$ can be attributed to −OH, C−O, O−H, and Ti−O bonds, respectively.[41,42] Additionally, compared with $Ti_3C_2T_x$, some new FT-IR peaks were observed in the spectrum of $NH_2-Ti_3C_2T_x$. For example, the peak at 1084 cm$^{-1}$ is attributed to the stretching vibration of the Si−O−C group, the peak at 1044 cm$^{-1}$ is attributed to the stretching vibration of the Si−O−Si group, and the peak at 879 cm$^{-1}$ is attributed to the stretching vibration of the Ti−O−Si group. Furthermore, characteristic FT-IR peaks at 1403 and 1214 cm$^{-1}$ can be observed, which are attributed to the bending vibration of the N−H bond and the stretching vibration of the C−N bond, respectively.[29] This analysis confirms the successful attachment of amino groups to the surface of $Ti_3C_2T_x$.

To understand the changes in the degree of carbon ordering in $NH_2-Ti_3C_2T_x$ after amino functionalization, Raman spectroscopy analysis was performed on $NH_2-Ti_3C_2T_x$, and the results are shown in Figure 2b. It can be observed that the Raman spectrum of $Ti_3C_2T_x$ contains four characteristic Raman peaks located at 191, 269, 400, and 572 cm$^{-1}$.[43] Similarly, the Raman spectrum of $NH_2-Ti_3C_2T_x$ also exhibits characteristic Raman peaks of $Ti_3C_2T_x$ within 700 cm$^{-1}$, which are located at 186, 280, 384, and 574 cm$^{-1}$. It is worth noting that the Raman spectrum of $NH_2-Ti_3C_2T_x$ shows a prominent D peak (1387 cm$^{-1}$) and G peak (1559 cm$^{-1}$), with an ID/IG ratio of 0.76, while the ID/IG ratio of unmodified $Ti_3C_2T_x$ is 0.63. Compared to unmodified $Ti_3C_2T_x$, $NH_2-Ti_3C_2T_x$ exhibits an increased ID/IG ratio, indicating that the originally ordered carbon structure in $Ti_3C_2T_x$ is disrupted after amino functionalization, leading to the formation of more amorphous carbon and an increase in the material's disorder.

$NH_2-Ti_3C_2T_x$ was characterized by using XRD to analyze its crystal structure, and the results are shown in Figure 2c. From the XRD spectrum, it can be observed that after etching
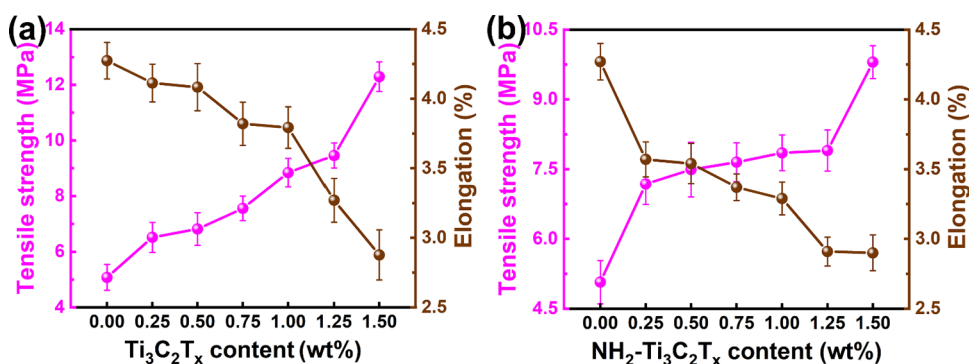
**Figure 4.** Mechanical performances of (a) TSPU and (b) NTSPU composites.
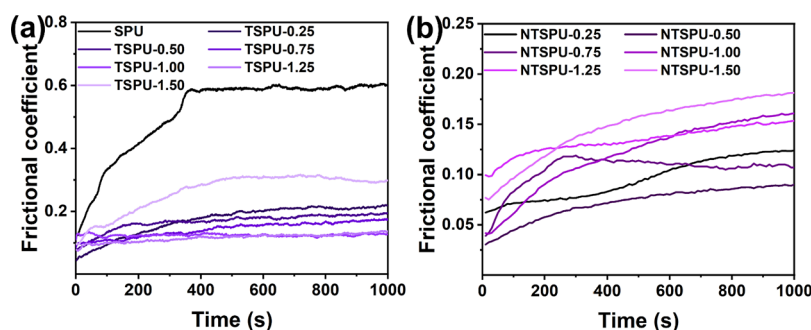


**Figure 5.** Friction curves of (a) TSPU and (b) NTSPU.

with hydrochloric acid and lithium fluoride, most of the characteristic peaks of the MAX phase disappear, and the (002) peak shifts to smaller angles, indicating the removal of the Al layer during etching.[43] Compared to unmodified $Ti_3C_2T_x$, the (002) peak of $NH_2-Ti_3C_2T_x$ shifts from 6.27° to 4.64° at a smaller angle, indicating an increased interlayer spacing due to the grafting of a large number of amino groups onto $Ti_3C_2T_x$.

The elemental chemical states of $NH_2-Ti_3C_2T_x$ were characterized by using XPS, as shown in Figure 2d. It can be observed that compared to unmodified $Ti_3C_2T_x$, $NH_2-Ti_3C_2T_x$ exhibits additional peaks in the N 1s, Si 2s, and Si 2p regions, confirming the presence of N and Si elements, which are the characteristic elements of $NH_2-Ti_3C_2T_x$. Therefore, amino functionalization of $Ti_3C_2T_x$ using APTES is successful, and a significant number of amino groups are chemically grafted onto the surface of $Ti_3C_2T_x$ through amino functionalization.

The microstructure of $Ti_3C_2T_x$ and $NH_2-Ti_3C_2T_x$ was characterized using SEM, and it was found that the densely stacked three-dimensional block-like MAX phase $Ti_3AlC_2$ transformed into accordion-like multilayered $Ti_3C_2T_x$ after chemical etching. From the images, it can be seen that $Ti_3C_2T_x$ exhibits an accordion-like multilayered structure. Compared to unmodified $Ti_3C_2T_x$, the surface of $NH_2-Ti_3C_2T_x$ appears rougher. This indicates that a significant number of amino groups are grafted onto the surface of $Ti_3C_2T_x$, forming a multilayered structure composed of multiple $NH_2-Ti_3C_2T_x$ layers.

*3.1.2. Compositions of PU-Based Composites.* In the FT-IR spectrum of SPU (Figure 3a), characteristic peaks can be observed at 1688, 1038, and 3318 $cm^{-1}$, corresponding to the stretching vibrations of carbonyl (-C = O) groups, sulfonic acid ($-SO_3H$) groups, and N−H groups. This indicates that the

sample successfully grafted sulfonic acid groups. Figure 3b shows the XPS spectrum of the SPU matrix, where peaks at 152, 284, 398, and 531 eV can be observed, corresponding to the S 2p, C 1s, N 1s, and O 1s peaks in the sulfonic acid groups.[43,44] The presence of the S 2p peak further confirms the successful grafting of sulfonic acid groups and the preparation of the zwitterionic polyurethane.

**3.2. Mechanical Performances of TSPU Composites.** The mechanical properties of materials are typically evaluated based on two parameters: tensile strength and elongation at break. Figure 4a presents the mechanical performances of SPU and TSPU samples. The SPU without $Ti_3C_2T_x$ exhibits a tensile strength of 5.05 MPa and an elongation at a break of 447%. As the $Ti_3C_2T_x$ content increases, the tensile strength of the $Ti_3C_2T_x$/SPU composite films gradually increases, while the elongation at break decreases. When the $Ti_3C_2T_x$ content is 1.25 wt %, the composite film material demonstrates excellent comprehensive mechanical properties, with a tensile strength of 9.46 MPa, which is 87.3% higher than that of SPU, and an elongation at break of 327%, which is 26.84% lower than that of SPU. This is mainly attributed to the interaction between the surface functional groups (−O, −F, −OH) of $Ti_3C_2T_x$ and the −NH− and C═O groups on SPU. With an increase in $Ti_3C_2T_x$ content, the hydrogen bonding interaction strengthens, limiting the mobility of the polymer chains and reducing their flexibility.[39] Additionally, the addition of $Ti_3C_2T_x$ inhibits the crystallization of the hard segments of the SPU molecular chains. However, due to the poor interfacial compatibility between $Ti_3C_2T_x$ and the SPU matrix, the introduction of $Ti_3C_2T_x$ also introduces a certain number of defects, leading to a decrease in elongation at break.

Similar trends can also be observed in the NTSPU system (Figure 4b). As the $NH_2-Ti_3C_2T_x$ content increases, the tensile strength of the composite film material gradually

increases. When the $NH_2-Ti_3C_2T_x$ content is 0.50 wt %, the tensile strength of the material increases to 7.49 MPa, which is 47.73% higher than that of SPU without $NH_2-Ti_3C_2T_x$. When the $NH_2-Ti_3C_2T_x$ content reaches 1.50 wt %, the tensile strength of the composite film material reaches 9.80 MPa, which is 93.29% higher than that of SPU. At the same time, as the $NH_2-Ti_3C_2T_x$ content increases, the elongation at the break of the material gradually decreases. This is mainly due to the interaction between the abundant $-NH_2$, $-OH$ groups on the surface of $NH_2-Ti_3C_2T_x$ and the N and H atoms in the SPU matrix, forming hydrogen bonds. With an increase in the $NH_2-Ti_3C_2T_x$ content, the hydrogen bonding interaction strengthens, hindering the internal rotation of the polymer chains and reducing their flexibility. Additionally, the presence of $NH_2-Ti_3C_2T_x$ hinders the movement of SPU molecular chains between the layers, limiting the elongation of the chains. However, the amino-functionalized NTSPU film, due to the presence of a higher content of silane oxide groups, increases the content of the soft segment in the system and enhances the interaction between the soft segments. Compared to the TSPU system, the NTSPU system exhibits lower chain flexibility and tensile strength.

### 3.3. Tribological Performances and Wear Mechanisms of TSPU Composites.

*3.3.1. Tribology Behavior.* The frictional behavior of TSPU and NTSPU was tested and the results are shown in Figure 5 and Table 1. From Figure 5a, it

**Table 1. Average Frictional Coefficient of SPU, TSPU, and NTSPU**

| MXene content (wt %) | SPU | TSPU | NTSPU |
|---|---|---|---|
| 0 | 0.52 ± 0.022 | | |
| 0.25 | | 0.17 ± 0.016 | 0.15 ± 0.012 |
| 0.50 | | 0.17 ± 0.010 | 0.11 ± 0.004 |
| 0.75 | | 0.14 ± 0.006 | 0.12 ± 0.006 |
| 1.00 | | 0.13 ± 0.006 | 0.17 ± 0.005 |
| 1.25 | | 0.12 ± 0.016 | 0.19 ± 0.003 |
| 1.50 | | 0.26 ± 0.006 | 0.22 ± 0.004 |

can be observed that SPU has a relatively high friction coefficient and a longer running-in period, with an average friction coefficient of 0.516. When a small amount of $Ti_3C_2T_x$ is added to SPU, the running-in period of the friction coefficient curve is shortened and the stability is improved. As the $Ti_3C_2T_x$ content increases, the friction coefficient of the material gradually decreases. When the $Ti_3C_2T_x$ content is 1.25 wt %, the composite film material exhibits the lowest average friction coefficient of 0.12 ± 0.016. However, when the $Ti_3C_2T_x$ mass fraction increases to 1.50 wt %, the friction coefficient of the $Ti_3C_2T_x$/SPU composite film material increases again, with an average coefficient of 0.26 ± 0.006, but this value is still lower than that of SPU. The lower friction coefficient is mainly attributed to the enhanced lubrication performance of the composite film material due to the relative sliding between the $Ti_3C_2T_x$ layers during friction. However, when the $Ti_3C_2T_x$ content is high, the agglomeration phenomenon severely affects the interfacial bonding strength between $Ti_3C_2T_x$ and SPU, leading to easy detachment during friction and a decrease in its friction-reducing performance.

In the NTSPU system (Figure 5b), it was found that when a small amount of $NH_2-Ti_3C_2T_x$ is added, the running-in period of the friction coefficient curve is shortened and the stability is

improved. As the $NH_2-Ti_3C_2T_x$ content increases, the friction coefficient of the material gradually decreases. When the $NH_2-Ti_3C_2T_x$ content is 0.50 wt %, the material exhibits the lowest average friction coefficient of 0.11 ± 0.004. However, when the $NH_2-Ti_3C_2T_x$ content reaches 0.75 wt %, the friction coefficient of the $NH_2-Ti_3C_2T_x$/SPU composite film material increases again. When the $NH_2-Ti_3C_2T_x$ content increases to 1.50 wt %, the friction coefficient of the $NH_2-Ti_3C_2T_x$/SPU composite film material reaches its maximum value of 0.22 ± 0.004, but this value is still lower than that of SPU. The composite film material exhibits lower and more stable friction coefficients when the $NH_2-Ti_3C_2T_x$ content is below 0.75 wt %. This is mainly attributed to the improved interfacial interaction between $NH_2-Ti_3C_2T_x$ and the matrix due to amino functionalization. During friction, the relative sliding between the $NH_2-Ti_3C_2T_x$ layers enhances the lubrication performance of the composite film material. The addition of amino-functionalized $Ti_3C_2T_x$ to SPU results in a relatively low friction coefficient. This is also due to the involvement of a large number of silane oxide groups in the soft segment of the SPU molecular network, which reduces the cohesive energy of the polymer itself and enhances the lubrication effect of the system.

*3.3.2. Wear Resistance.* From Figure 6a, it can be seen that the wear rate of SPU is the highest, reaching 21.18 × $10^{-3}$ mm$^3$/(Nm). Compared to SPU, the wear rates of TSPU composite films containing $Ti_3C_2T_x$ are all reduced, and they show a trend of first decreasing and then increasing, consistent with the trend of the friction coefficient. With the increase of $Ti_3C_2T_x$ content, the wear rate of the composite film material gradually decreases, and when the $Ti_3C_2T_x$ content is 1.25 wt %, the wear rate of the material is the lowest, at 3.68 × $10^{-3}$ mm$^3$/(Nm). When the mass fraction of $Ti_3C_2T_x$ increases to 1.50 wt %, the wear rate of the composite film material also increases, reaching 12.13 × $10^{-3}$ mm$^3$/(Nm), but still lower than the wear rate of SPU. This is because adding $Ti_3C_2T_x$ to the SPU matrix can deflect the crack path, and hinder the rapid propagation of microcracks in the composite film material, thereby inhibiting the formation of wear debris during the wear process and reducing the wear rate of the material. However, excessive $Ti_3C_2T_x$ in the SPU matrix can cause aggregation, making cracks easy to propagate, thereby affecting its antiwear effect in the matrix. From the surface morphology of the wear track (Figure 6c), it can also be seen that SPU is severely damaged during the friction process, resulting in a rough wear surface and partial film around the wear track, reflecting severe plastic deformation. This indicates that $Ti_3C_2T_x$ participates in the friction and wear process, promoting the formation of transfer films in the friction contact area and slowing down the shearing action of the friction pair on SPU.

Similar results can also be observed in the NTSPU system (Figure 7b,d). When the $NH_2-Ti_3C_2T_x$ content is 0.50 wt %, the wear rate of the material reaches its lowest value, only 4.7 × $10^{-4}$ mm$^3$/(Nm). When the $NH_2-Ti_3C_2T_x$ content continues to increase to 1.50 wt %, the wear rate of the $NH_2-Ti_3C_2T_x$/SPU composite film material reaches its maximum value, at 4.91 × $10^{-3}$ mm$^3$/(Nm), but this value is still lower than the wear rate of SPU. This is mainly because, after amino modification treatment of $Ti_3C_2T_x$, the $NH_2-Ti_3C_2T_x$ surface is enriched with amino functional groups, which can enhance its interface interaction with the SPU matrix, thereby improving the dispersion of $NH_2-Ti_3C_2T_x$ in the SPU matrix. Uniformly dispersed $NH_2-Ti_3C_2T_x$ can
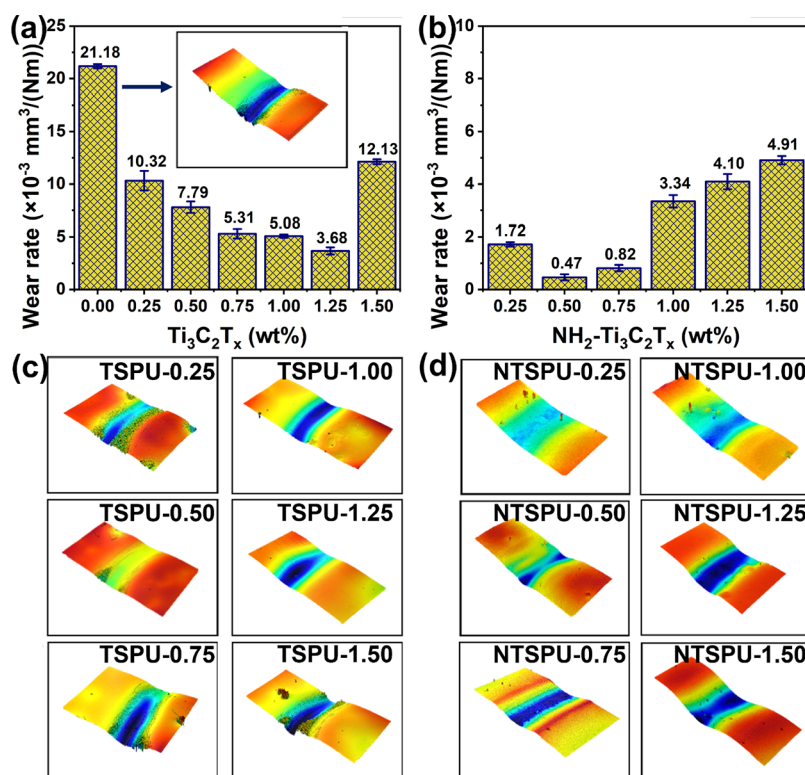
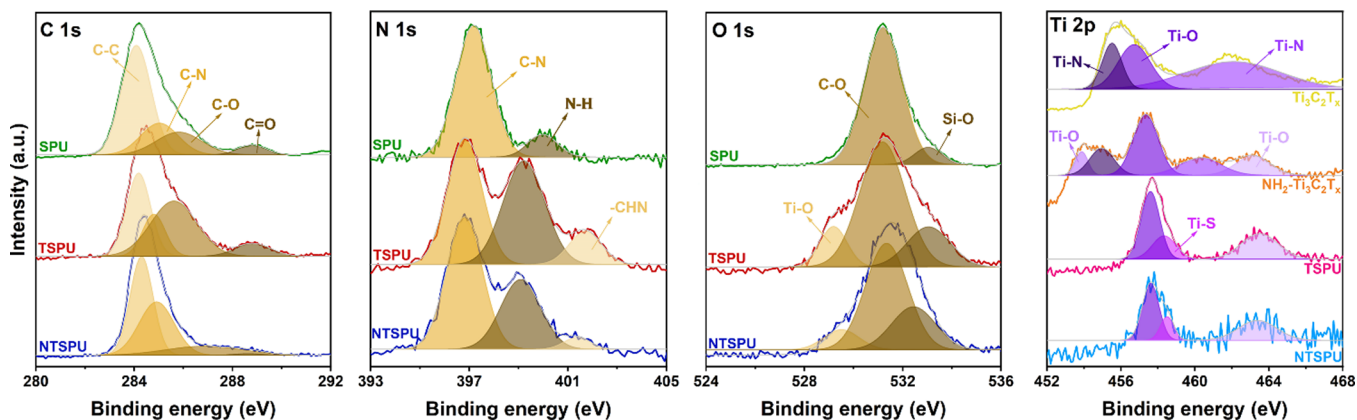**Figure 6.** (a,b) Wear ratio and (c,d) 3D morphology. (a,c) TSPU and (b,d) NTSPU.



**Figure 7.** XPS spectra of the rubbed wafer. (C) C 1s, N 1s, and O 1s spectra contain SPU, TSPU, and NTSPU. Ti 2p spectra contain $Ti_3C_2T_x$, $NH_2-Ti_3C_2T_x$, TSPU, and NTSPU.

deflect crack paths and hinder the propagation of microcracks in the composite film material, thereby reducing the formation of wear debris and lowering the wear rate of the material. However, excessive $NH_2-Ti_3C_2T_x$ can still undergo slight aggregation, making cracks more prone to propagation, thereby affecting the full play of its antiwear effect. The addition of $NH_2-Ti_3C_2T_x$ can effectively reduce the wear scar area of the material, making the wear interface relatively smooth and thereby reducing the wear rate.

*3.3.3. Surface Chemistry.* To further investigate the chemical states of the transfer films on samples SPU, TSPU-1.25, and NTSPU-0.50 and analyze their formation mechanisms, XPS characterization analysis was performed on the transfer films of the samples, as shown in Figure 7. In the fine spectrum of C 1s of SPU, fitting reveals the presence of C−C, C−N, C−O, and C═O bonds, located at 284.1 285.0, 285.8,

and 288.8 eV, respectively. After the addition of $Ti_3C_2T_x$, it was found that the C−O and C═O peaks in the TSPU spectrum were significantly enhanced. This indicates that $Ti_3C_2T_x$ provides more active sites for frictional chemical reactions and self-repair during the friction process, which is beneficial for the lubrication and self-repair of the polymer film. When $NH_2-Ti_3C_2T_x$ is added, the C−N peak is significantly enhanced, which also proves the involvement of $NH_2-Ti_3C_2T_x$ in the friction process.

In the fine spectrum of SPU with N 1s, only the C−N peak (397.2 eV) and N−H peak (380.0 eV) on the polymer molecular chain were found after the addition of $Ti_3C_2T_x$ and $NH_2-Ti_3C_2T_x$, and the −CHN peak (401.7 eV) appeared in both TSPU and NTSPU spectra. This indicates that the addition of two-dimensional materials enhances the interfacial chemical activity, facilitating lubrication implementation.
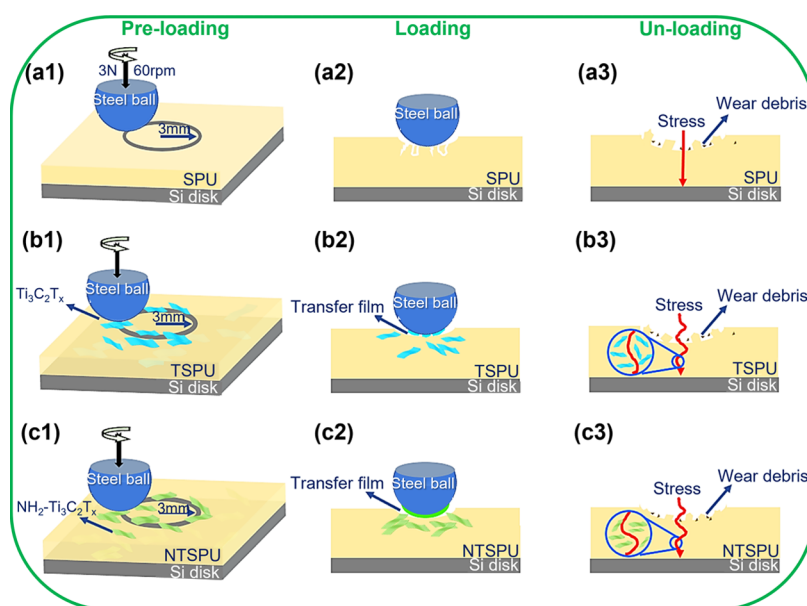
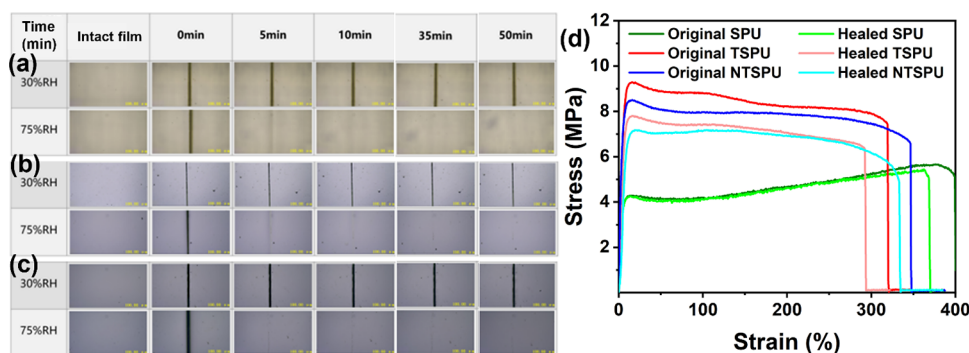**Figure 8.** Wear mechanisms of (a) SPU, (b) TSPU, and (c) NTSPU.



**Figure 9.** Self-healing Performances of SPU, TSPU, and NTSPU. (a−c) A self-healing process under 30%RH and 75%RH humidity. (a) SPU, (b) TSPU, and (c) NTSPU. (d) Stress−strain curves under 75%RH humidity at 20 °C.

In SPU, the O 1s spectrum can be fitted into two peaks located at 531.2 and 533.0 eV, which are attributed to the C−O bond and Si−O bond, respectively. The presence of the Si−O bond indicates that the surface of $Si_3N_4$ spheres is oxidized and partially detached, thereby participating in the formation of the transfer film. With the addition of $Ti_3C_2T_x$ and $NH_2−Ti_3C_2T_x$, the Ti−O peak (529.1 eV) appears, confirming the involvement of $Ti_3C_2T_x$ and $NH_2−Ti_3C_2T_x$ in the formation of the friction transfer film.

In the fine spectrum of $Ti_3C_2T_x$ in Ti 2p, there are Ti−O bonds (458.3 eV) and Ti−N bonds (463.5 and 457.6 eV). However, after friction of the TSPU film, a Ti−S peak (458.2 eV) appears on the surface. This indicates that during the friction process frictional chemical reactions occur between $Ti_3C_2T_x$ and the sulfonic acid groups in the polymer matrix, resulting in the formation of Ti−S bonds. This is consistent with the changes in the Ti peak in the NTSPU spectrum.

*3.3.4. Wear Mechanisms.* To summarize the lubrication mechanism of $Ti_3C_2T_x$/SPU composite film materials, a schematic diagram of the friction model and a schematic diagram of the wear cross-section of SPU and its composite film materials were drawn, as shown in Figure 8. Under shear stress, the $Ti_3C_2T_x$/SPU composite film material forms a lubricating transfer film on the surface of the wear track. On

the one hand, this transfer film acts as a lubricant due to the weak van der Waals forces between the $Ti_3C_2T_x$ layers, allowing for easy sliding between the layers under external forces, thus achieving lubrication. On the other hand, the $Ti_3C_2T_x$ lubricating transfer film also acts as a support, effectively reducing the direct contact between the shear stress and the composite film material, thereby reducing the friction coefficient and wear rate of the material. Additionally, when $Ti_3C_2T_x$ is added to the SPU matrix, it acts as a barrier, making the path of external force more tortuous and slowing the crack propagation speed. Therefore, by adding an optimal amount of $Ti_3C_2T_x$ to the SPU matrix, it can simultaneously reduce friction and wear, thereby improving the lubrication performance and wear resistance of the composite film material.

During the friction process, the $NH_2−Ti_3C_2T_x$/SPU composite film material forms a transfer film mainly composed of $NH_2−Ti_3C_2T_x$ on the surface of the wear track due to shear stress, effectively reducing the friction coefficient and wear rate. Compared to the transfer film of $Ti_3C_2T_x$/SPU composite film material, the transfer film of the $NH_2−Ti_3C_2T_x$/SPU composite film material is denser and more continuous. In comparison, the $Ti_3C_2T_x$ transfer film is relatively thinner and less continuous. This is because the nonreactive nature of the $Ti_3C_2T_x$ surface results in weak interfacial interactions between

$Ti_3C_2T_x$ and the SPU matrix. In contrast, the $NH_2-Ti_3C_2T_x$ surface contains a large number of amino groups, which provide stronger interfacial interactions with the SPU matrix, thereby imparting the $NH_2-Ti_3C_2T_x$/SPU composite film material with the ability to resist plastic deformation and microcracking. Additionally, the amino functionalization allows $NH_2-Ti_3C_2T_x$ to distribute more uniformly in the SPU matrix, reducing the occurrence of aggregation and stress concentration while also reducing friction and wear, ultimately improving the lubrication performance and wear resistance of the composite film material.

### 3.4. Self-Healing Performances of TSPU Composites.

Endowing materials with excellent self-healing properties can extend their service life. Generally, the self-healing performance of materials can be manifested from two aspects: microscale self-healing and mechanical self-healing. Microscale self-healing can be observed by microscopy to observe the healing process of samples (Figure 9). It can be observed that under 30%RH humidity conditions, the samples of SPU, TSPU-1.25, and NTSPU-0.50 are not able to heal completely, while under 75%RH and 20 °C conditions, the incisions of SPU, TSPU-1.25, and NTSPU-0.50 samples spontaneously heal until the incisions disappear. Moreover, it can be noticed that under 75%RH humidity conditions, the cut samples are visibly healed after only 5 min of repair, and as the repair time extends, the incisions become less and less noticeable until they disappear completely. This is because in a humid environment, the -NH- groups and $-SO_3H$ groups in the damaged interface of the SPU matrix can move to the damaged interface through hydration, and the zwitterionic structure at the two damaged interfaces achieves self-healing through the combined action of hydration and weak electrostatic forces.

The stress−strain curves of the initial and healed samples of SPU, TSPU-1.25, and NTSPU-0.50 are shown in Figure 9d. Under 75%RH humidity conditions, the self-healing efficiency of SPU samples reaches 95.7%, while the self-healing efficiency of TSPU is 83.9% and that of NTSPU is 84.4%. SPU matrix exhibits excellent humidity-sensitive self-healing performance. The composite film materials with a small amount of $Ti_3C_2T_x$ still possess excellent self-healing properties, but their self-healing efficiency is slightly lower compared with SPU. This may be attributed to the shielding effect of the introduced layered $Ti_3C_2T_x$ structure on the interaction of zwitterionic groups in the SPU matrix. However, after the amino functionalization of $Ti_3C_2T_x$, more active sites of zwitterionic groups are provided, thereby enhancing the self-repair capability of the composite film.

## 4. CONCLUSIONS

Self-healing PU is an excellent matrix material that can significantly prolong the lifespan of composite materials. Meanwhile, $Ti_3C_2T_x$ with a layered structure exhibits relatively weak interlayer van der Waals forces, which allows it to undergo slip when subjected to friction. In this study, SPU was synthesized using a simple two-step method. $Ti_3C_2T_x$ was prepared by an in situ etching method and then chemically modified with a silane coupling agent APTES to obtain $NH_2-Ti_3C_2T_x$ to provide a large amount of self-healing active points. Finally, $NH_2-Ti_3C_2T_x$ was combined with SPU to obtain the NTSPU composite film material, which possesses excellent lubrication and self-healing properties via cooperating self-healing PU and modified $Ti_3C_2T_x$. The maximum tensile strength of the film material can reach 9.80 MPa, which is

93.29% higher than that of a pure SPU matrix. Under 75%RH and 20 °C conditions, the scratch of the composite film material can heal in as fast as 5 min, with a self-healing efficiency of 84.4%. At the same time, the friction coefficient of the NTSPU composite film material is as low as 0.11, and the wear rate reaches $4.7 \times 10^{-4}$ mm$^3$/(Nm), which is reduced by 79.7 and 97.8% compared to SPU, respectively. Due to the abundant amino and silane oxygen groups on the surface of $NH_2-Ti_3C_2T_x$, it exhibits stronger interfacial adhesion and matrix dispersion with the matrix, thereby endowing good self-healing and tribological performances in actuating the part surface.

## ■ AUTHOR INFORMATION

### Corresponding Authors

**Chunpeng Chai** − *School of Materials Science and Engineering, Beijing Institute of Technology, Beijing 100081, China*; Email: chaicp@bit.edu.cn

**Haosheng Pang** − *Chinese Aeronautical Establishment, Beijing 100012, China; State Key Laboratory of Tribology in Advanced Equipment, Department of Mechanical Engineering, Tsinghua University, Beijing 100084, China;* orcid.org/0000-0001-9505-7664; Email: panghs.2020@tsinghua.org.cn

### Authors

**Zhenqian Ma** − *School of Materials Science and Engineering, Beijing Institute of Technology, Beijing 100081, China*

**Xuan Yin** − *College of Mechanical and Electrical Engineering, Beijing University of Chemical Technology, Beijing 100029, China;* orcid.org/0000-0003-3249-9814

Complete contact information is available at:
https://pubs.acs.org/10.1021/acsapm.3c02629

### Notes

The authors declare no competing financial interest.

## ■ REFERENCES

(1) Zhang, Z.; Wang, L.; Yu, H.; Zhang, F.; Tang, L.; Feng, Y.; Feng, W. Highly Transparent, Self-Healable, and Adhesive Organogels for Bio-Inspired Intelligent Ionic Skins. *ACS Appl. Mater. Interfaces* **2020**, *12* (13), 15657−15666.

(2) Yin, X.; Jin, J.; Chen, X.; Rosenkranz, A.; Luo, J. Ultra-Wear-Resistant MXene-Based Composite Coating via in Situ Formed Nanostructured Tribofilm. *ACS Appl. Mater. Interfaces* **2019**, *11* (35), 32569−32576.

(3) Tang, Z.; Li, S. A review of recent developments of friction modifiers for liquid lubricants (2007-present). *Curr. Opin. Solid State Mater. Sci.* **2014**, *18* (3), 119−139.

(4) Yin, X.; Jin, J.; Chen, X.; Ma, T.; Zhang, C. A New Pathway for Superlubricity in a Multilayered MoS2-Ag Film under Cryogenic Environment. *Nano Lett.* **2021**, *21* (24), 10165−10171.

(5) Jin, B.; Zhao, J.; Chen, G.; He, Y.; Huang, Y.; Luo, J. In situ synthesis of $Mn_3O_4$/graphene nanocomposite and its application as a lubrication additive at high temperatures. *Appl. Surf. Sci.* **2021**, *546*, No. 149019.

(6) Bat-Erdene, M.; Batmunkh, M.; Sainbileg, B.; Hayashi, M.; Bati, A. S. R.; Qin, J.; Zhao, H.; Zhong, Y. L.; Shapter, J. G. Highly Dispersed Ru Nanoparticles on Boron-Doped $Ti_3C_2T_x$ (MXene) Nanosheets for Synergistic Enhancement of Electrocatalytic Hydrogen Evolution. *Small* **2021**, *17* (38), No. 2102218.

(7) Zhao, J.; Li, Y.; He, Y.; Luo, J. In Situ Green Synthesis of the New Sandwichlike Nanostructure of $Mn_3O_4$/Graphene as Lubricant Additives. *ACS Appl. Mater. Interfaces* **2019**, *11* (40), 36931−36938.

(8) Gong, D.; Xue, Q.; Wang, H. Study of the wear of filled polytetrafluoroethylene. *Wear* **1989**, *134*, 283−295.

(9) Blanchet, T. A.; Kennedy, F. E. Sliding wear mechanism of polytetrafluoroethylene and PTFE composites. *Wear* **1992**, *153*, 229−243.

(10) Wu, X.; Zhang, Y.; Du, P.; Jin, Z.; Zhao, H.; Wang, L. Synthesis, characterization and properties of graphene-reinforced polyimide coatings. *New J. Chem.* **2019**, *43* (15), 5697−5705.

(11) Yuan, H.; Yang, S.; Liu, X.; Wang, Z.; Ma, L.; Hou, K.; Yang, Z.; Wang, J. Polyimide-based lubricating coatings synergistically enhanced by $MoS_2$@HCNF hybrid. *Composites Part A: Applied Science and Manufacturing* **2017**, *102*, 9−17.

(12) Pan, B.; Zhao, J.; Zhang, Y.; Zhang, Y. Wear Performance and Mechanisms of Polyphenylene Sulfide/Polytetrafluoroethylene Wax Composite Coatings Reinforced by Graphene. *Journal of Macromolecular Science, Part B* **2012**, *51* (6), 1218−1227.

(13) Yin, X.; Zhang, J.; Luo, T.; Cao, B.; Xu, J.; Chen, X.; Luo, J. Tribochemical mechanism of superlubricity in graphene quantum dots modified DLC films under high contact pressure. *Carbon* **2021**, *173*, 329−338.

(14) Verma, P. C.; Ciudin, R.; Bonfanti, A.; Aswath, P.; Straffelini, G.; Gialanella, S. Role of the friction layer in the high-temperature pin-on-disc study of a brake material. *Wear* **2016**, *346−347*, 56−65.

(15) Keshavamurthy, R.; Tambrallimath, V.; Rajhi, A. A.; R, M. S.; Patil, A. Y.; Yunus Khan, T. M.; Makannavar, R. Influence of Solid Lubricant Addition on Friction and Wear Response of 3D Printed Polymer Composites. *Polymers* **2021**, *13* (17), 2905.

(16) Zhang, Y.; Hourston, D. J. Rigid Interpenetrating Polymer Network Foams Prepared from a Rosin-Based Polyurethane and an Epoxy Resin. *J. Appl. Polym. Sci.* **1998**, *69*, 271−281.

(17) Mao, L.; Jiao, Y.; Geng, H.; Tang, Y. Understanding friction and wear properties of carbon fiber/epoxy stitched composites. *Composites Part A: Applied Science and Manufacturing* **2023**, *169*, No. 107501.

(18) Zhai, W. Z.; Bai, L. C.; Zhou, R. H.; Fan, X. L.; Kang, G. Z.; Liu, Y.; Zhou, K. Recent Progress on Wear-Resistant Materials: Designs, Properties, and Applications. *Adv. Sci.* **2021**, *8* (11), No. e2003739.

(19) Mo, M.; Zhao, W.; Chen, Z.; Yu, Q.; Zeng, Z.; Wu, X.; Xue, Q. Excellent tribological and anti-corrosion performance of polyurethane composite coatings reinforced with functionalized graphene and graphene oxide nanosheets. *RSC Adv.* **2015**, *5* (70), 56486−56497.

(20) Song, H.-J.; Zhang, Z.-Z. Investigation of the tribological properties of polyfluo wax/polyurethane composite coating filled with nano-SiC or nano-$ZrO_2$. *Materials Science and Engineering: A* **2006**, *426* (1−2), 59−65.

(21) Song, H.-J.; Zhang, Z.-Z.; Men, X.-H.; Luo, Z.-Z. A study of the tribological behavior of nano-ZnO-filled polyurethane composite coatings. *Wear* **2010**, *269* (1−2), 79−85.

(22) Wang, M.; Wang, Z.; Chen, Q.; Meng, X.; Heng, L. Preparation of Polyurethane/Graphite Composite Films with Stable Mechanical Property and Wear Resistance Underwater. *J. Nanosci. Nanotechnol.* **2018**, *18* (6), 4349−4354.

(23) Xu, J.; Li, Y.; Liu, T.; Wang, D.; Sun, F.; Hu, P.; Wang, L.; Chen, J.; Wang, X.; Yao, B.; Fu, J. Room-Temperature Self-Healing Soft Composite Network with Unprecedented Crack Propagation Resistance Enabled by a Supramolecular Assembled Lamellar Structure. *Adv. Mater.* **2023**, *35* (26), No. e2300937.

(24) Yu, H.; Chen, C.; Sun, J.; Zhang, H.; Feng, Y.; Qin, M.; Feng, W. Highly Thermally Conductive Polymer/Graphene Composites with Rapid Room-Temperature Self-Healing Capacity. *Nano-Micro Lett.* **2022**, *14* (1), 135.

(25) Zhang, Z.; Tang, L.; Chen, C.; Yu, H.; Bai, H.; Wang, L.; Qin, M.; Feng, Y.; Feng, W. Liquid metal-created macroporous composite hydrogels with self-healing ability and multiple sensations as artificial flexible sensors. *Journal of Materials Chemistry A* **2021**, *9* (2), 875−883.

(26) Bai, H.; Zhang, Z.; Huo, Y.; Shen, Y.; Qin, M.; Feng, W. Tetradic double-network physical crosslinking hydrogels with synergistic high stretchable, self-healing, adhesive, and strain-sensitive properties. *Journal of Materials Science & Technology* **2022**, *98*, 169−176.

(27) Ma, J.; Yang, Y.; Valenzuela, C.; Zhang, X.; Wang, L.; Feng, W. Mechanochromic, Shape-Programmable and Self-Healable Cholesteric Liquid Crystal Elastomers Enabled by Dynamic Covalent Boronic Ester Bonds. *Angew. Chem., Int. Ed.* **2022**, *61* (9), No. e202116219.

(28) Olugebefola, S. C.; Hamilton, A. R.; Fairfield, D. J.; Sottos, N. R.; White, S. R. Structural reinforcement of microvascular networks using electrostatic layer-by-layer assembly with halloysite nanotubes. *Soft Matter* **2014**, *10* (4), 544−548.

(29) Billiet, S.; Hillewaere, X. K.; Teixeira, R. F.; Du Prez, F. E. Chemistry of crosslinking processes for self-healing polymers. *Macromol. Rapid Commun.* **2013**, *34* (4), 290−309.

(30) Zheng, L.; Sundaram, H. S.; Wei, Z.; Li, C.; Yuan, Z. Applications of zwitterionic polymers. *React. Funct. Polym.* **2017**, *118*, 51−61.

(31) Li, Y.; Meng, F.; Mei, Y.; Wang, H.; Guo, Y.; Wang, Y.; Peng, F.; Huang, F.; Zhou, Z. Electrospun generation of $Ti_3C_2T_x$ MXene@ graphene oxide hybrid aerogel microspheres for tunable high-performance microwave absorption. *Chemical Engineering Journal* **2020**, *391*, No. 123512.

(32) Lipatov, A.; Lu, H.; Alhabeb, M.; Anasori, B.; Gruverman, A.; Gogotsi, Y.; Sinitskii, A. Elastic properties of 2D $Ti_3C_2T_x$ MXene monolayers and bilayers. *Sci. Adv.* **2018**, *4* (6), No. eaat0491.

(33) Serles, P.; Hamidinejad, M.; Demingos, P. G.; Ma, L.; Barri, N.; Taylor, H.; Singh, C. V.; Park, C. B.; Filleter, T. Friction of $Ti_3C_2T_x$ MXenes. *Nano Lett.* **2022**, *22* (8), 3356−3363.

(34) Yin, X.; Pang, H.; Xu, J.; Liu, D.; Chai, C.; Zhang, B. In Situ-Formed Ultralow Wear Tribofilms Induced by Poly(Acrylic Acid)-co-MXene-Modified Polymer-Like Carbon Films. *Adv. Eng. Mater.* **2022**, *24* (7), No. 2101661.

(35) Yan, H.; Zhang, L.; Li, H.; Fan, X.; Zhu, M. Towards high-performance additive of $Ti_3C_2$/graphene hybrid with a novel wrapping structure in epoxy coating. *Carbon* **2020**, *157*, 217−233.

(36) Shen, S.; Ke, T.; Rajavel, K.; Yang, K.; Lin, D. Dispersibility and Photochemical Stability of Delaminated MXene Flakes in Water. *Small* **2020**, *16* (36), No. e2002433.

(37) Hao, L.; Zhang, H.; Wu, X.; Zhang, J.; Wang, J.; Li, Y. Novel thin-film nanocomposite membranes filled with multi-functional $Ti_3C_2T_x$ nanosheets for task-specific solvent transport. *Composites Part A: Applied Science and Manufacturing* **2017**, *100*, 139−149.

(38) Yin, X.; Chen, H.; Jiang, L.; Liang, C.; Pang, H.; Liu, D.; Zhang, B. Effects of polyacrylic acid molecular weights on $V_2C$-MXene nanocoatings for obtaining ultralow friction and ultralow wear in an ambient working environment. *Phys. Chem. Chem. Phys.* **2022**, *24* (44), 27406−27412.

(39) Yan, H.; Fan, X.; Cai, M.; Song, S.; Zhu, M. Amino-functionalized $Ti_3C_2T_x$ loading ZIF-8 nanocontainer@benzotriazole as multifunctional composite filler towards self-healing epoxy coating. *J. Colloid Interface Sci.* **2021**, *602*, 131−145.

(40) He, D.; Cai, M.; Yan, H.; Lin, Q.; Fan, X.; Zhang, L.; Zhu, M. Tribological properties of $Ti_3C_2T_x$ MXene reinforced interpenetrating polymers network coating. *Tribol. Int.* **2021**, *163*, No. 107196.

(41) Cai, M.; Yan, H.; Song, S.; He, D.; Lin, Q.; Li, W.; Fan, X.; Zhu, M. State-of-the-art progresses for $Ti_3C_2T_x$ MXene reinforced polymer composites in corrosion and tribology aspects. *Adv. Colloid Interface Sci.* **2022**, *309*, No. 102790.

(42) Wang, H.-W.; Naguib, M.; Page, K.; Wesolowski, D. J.; Gogotsi, Y. Resolving the Structure of $Ti_3C_2T_x$ MXenes through Multilevel Structural Modeling of the Atomic Pair Distribution Function. *Chem. Mater.* **2016**, *28* (1), 349−359.

(43) Zhang, L.; Su, W.; Huang, Y.; Li, H.; Fu, L.; Song, K.; Huang, X.; Yu, J.; Lin, C.-T. In Situ High-Pressure X-ray Diffraction and Raman Spectroscopy Study of $Ti_3C_2T_x$ MXene. *Nanoscale Res. Lett.* **2018**, *13*, 343.

(44) Zuo, T.; Xie, C.; Wang, W.; Yu, D. $Ti_3C_2T_X$ MXene-Ferroferric Oxide/Carbon Nanotubes/Waterborne Polyurethane-Based Asymmetric Composite Aerogels for Absorption-Dominated Electromagnetic Interference Shielding. *ACS Applied Nano Materials* **2023**, *6* (6), 4716−4725.